

Ultrafast Flash Energy Conductance at MXene-Surfactant Interface and Its Molecular Origins

Jiebo Li, Qi Zhang, Li Yan, Guorong Wu, Mingjun Hu,* Xubo Lin,* Kaijun Yuan,* and Xueming Yang

With the developments of energy science, biomedical therapy, and electronic technology, interfacial thermal transport has become a key issue for many applications. Furthermore, with the growing importance of thermal utilization of new 2D material MXene, capturing the interfacial thermal conduction of MXene-soft material in solution is an urgent task. In this work, transient absorption dynamics is employed to investigate MXene ($\text{Ti}_3\text{C}_2\text{T}_x$)-surfactant interfacial energy conductance in water solution. The sodium dodecyl sulfate molecules could not directly interact with $\text{Ti}_3\text{C}_2\text{T}_x$ surface, and thus failed to inhibit the interfacial heat transfer of $\text{Ti}_3\text{C}_2\text{T}_x$. To the opposite, attributed to strong coulomb interaction, cetrimonium bromide (CTAB) molecules could form bilayers on $\text{Ti}_3\text{C}_2\text{T}_x$ to isolate the energy dissipation from $\text{Ti}_3\text{C}_2\text{T}_x$ to water and thus alter the heat dissipation rates of $\text{Ti}_3\text{C}_2\text{T}_x$. The interfacial energy conductance $G \approx 81 \text{ MW m}^{-2} \text{ K}^{-1}$ between CTAB and $\text{Ti}_3\text{C}_2\text{T}_x$ is quantitatively obtained. Molecular dynamics simulation also presented the flash heating could disrupt the bilayer structures, showing that the finding contributed to the future engineering design for MXene thermal applications through tuning the attaching layer at MXene interface.

from electronics,^[1] photonics,^[2] biomedical therapy,^[3] to thermal management,^[4,5] and energy storage.^[6] Knowledge about the interaction between surface molecules and nanomaterial is thus essential for a thorough understanding of the ways for energy conductance at interface.^[7] Furthermore, tuning these energy migration pathways could determine the applications of various systems.^[8] In these nanomaterials, due to the high-efficiency light-to-heat conversion ability, MXene ($\text{Ti}_3\text{C}_2\text{T}_x$) as a new type of 2D material with plasmonic property,^[9] is attracting growing interests in various applications,^[10] such as desalination,^[11] actuator,^[12] and photocatalysis.^[13] Particularly, because the absorption peak of MXene is located in the near infrared transparency window of biological tissues, this new 2D material can be exploited for applications in biomedical imaging,^[14]

drug delivery,^[15,16] and cancer therapy.^[17] As the fundamental knowledge of these applications, once the photon energy is absorbed by MXene, the electronic excitation is generated and eventually converted into thermal energy. The energy transport occurs through the interface layer that interacts with MXene to the local environment. Investigating the process of thermal transfer from MXene flakes through the interface layer to the environment is thus critical for utilizing MXene in many emerging areas, such as photothermal therapy, drug delivery, water stream, and bioimaging.

Such energy transport pathways are not only related with materials, but also be modulated by interfacial molecules. In pioneer's research, interfacial molecule has been demonstrated to be the limited step in thermal dissipation of nanotube-based composite.^[18] With employed gold as heating source, pioneer researchers have quantitatively investigated thermal conducting via carbon chain and heat transfer across hard-soft interface.^[19–22] Tuning the surface adhesions between surface molecules and materials from strong to weak could significantly slow down the rate of thermal conduction on material surface.^[23] Frequently, investigators are interested in heating surfactant layers in order to understand the energy migration at the interface.^[24–26] Surfactants are also widely used on MXene surface for various purposes, such as 3D structure assembling,^[27] mesopore-directing agent,^[28,29] and supercapacitor.^[30] Moreover, in the previous research, surfactant could be an effective surface

1. Introduction


With the development of nanotechnology, interfacial energy transport of nanoscale building block has become a key issue for fundamental physics and practical applications, ranging

Dr. J. Li, Dr. X. Lin
Beijing Advanced Innovation Center for Biomedical Engineering
School of Biological Science and Medical Engineering
Beihang University
Beijing 100191, China
E-mail: linxbseu@buaa.edu.cn

Q. Zhang, Prof. G. Wu, Prof. K. Yuan, Prof. X. Yang
State Key Laboratory of Molecular Reaction Dynamics
Dalian Institute of the Chemical Physics
Chinese Academy of Sciences
Dalian, Liaoning 116023, China
E-mail: kjyuan@dicp.ac.cn

Q. Zhang
University of Chinese Academy of Sciences
Beijing 100049, China

L. Yan, Dr. M. Hu
School of Materials Science and Engineering
Beihang University
Beijing 100191, China
E-mail: mingjunhu@buaa.edu.cn

 The ORCID identification number(s) for the author(s) of this article can be found under <https://doi.org/10.1002/admi.201901461>.

DOI: 10.1002/admi.201901461

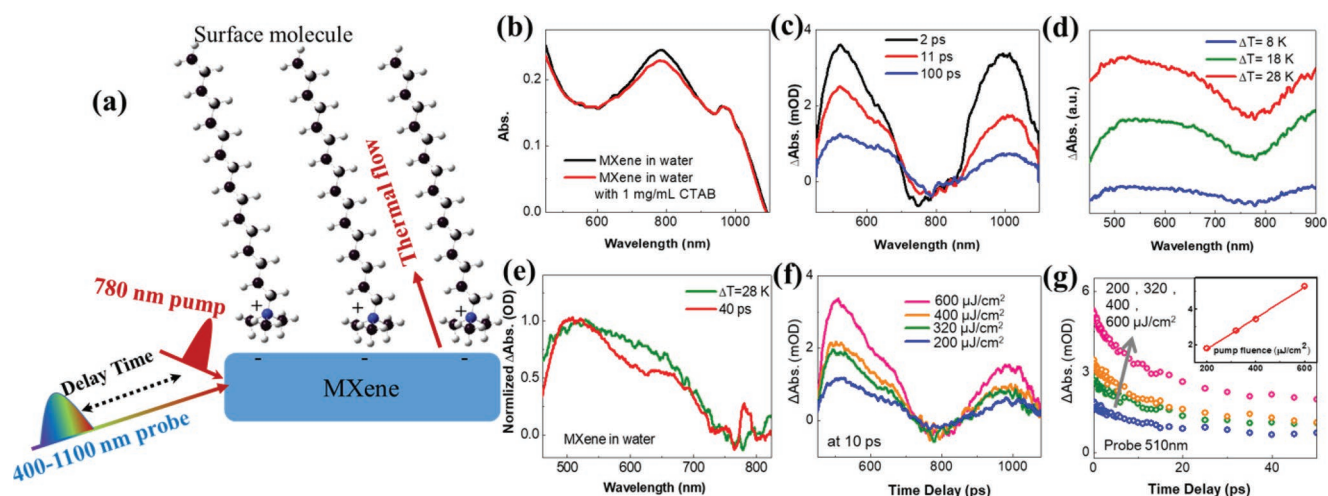


Figure 1. Ultrafast investigation of MXene in solution. a) Schematic diagram of ultrafast pump-probe for interfacial thermal transports, b) MXene visible spectrum in different solutions, c) time dependent spectrum of MXene in solution (0.05 mg mL^{-1}) under 780 nm excitation, d) temperature differences spectrum of MXene in water, e) comparison of temperature difference spectrum ($\Delta T = 28 \text{ K}$) with pump probe spectrum at 40 ps, f) pump fluence intensity dependence transition spectrum of MXene at 10 ps, g) pump intensities dependent dynamics.

protective agent to retard MXene's oxidation.^[31] Therefore, the investigation of energy transport from MXene through surfactant layer is not only fundamentally important as the model system for understanding photothermal conversion process, but also provides evidences for interfacial molecular interactions associated with many practical applications.

In this paper, to quantitatively gain the understanding of the interfacial energy migration pathways from MXene to surfactant molecules, we conducted a series of studies about interfacial energy flux dynamic processes by employing ultrafast spectroscopy. With the investigation of several typical surfactants, we found that cetrimonium bromide (CTAB) molecules could effectively block the energy transport from MXene to water due to strong coulomb interaction between CTAB and MXene. The additions of sodium dodecyl sulfate (SDS) and tetra methyl ammonium bromide (TMAB) molecules do not affect the heat dissipation of MXene significantly because of either weak interaction or short carbon chain length. The results indicated that the synergistic effect of strong bonding and hydrophobicity of surface attaching layer played a crucial role in obstructing the energy transfer from MXene to water. By quantitatively increasing the CTAB concentration, the MXene energy dissipation channels could be retarded. The trends transition occurred before the CTAB critical micelle concentration. The interfacial energy conduction G is $\approx 81 \text{ MW m}^{-2} \text{ K}^{-1}$. Molecular dynamic (MD) simulation provided the molecular insight of CTAB concentration dependent assembly at MXene surface. MD simulation also indicated that heating the MXene surface could perturb the bilayer structure of CTAB. Investigating the molecular origins and monitoring the heat flow from MXene under plasmonic excitation to interfacial surfactants could thus provide fundamental understanding and serve as a guide to the design of MXene systems for a desired photothermal application.

2. Results and Discussion

2.1. Ultrafast Spectroscopy Could Track the Energy Transport Pathway for MXene-Surfactant Interface

In the past two decades, transition absorption method is widely used for the measurements of thermal conductance in solution, even though it has some unavoidable drawbacks.^[7] Thus, the ultrafast optical pump-probe technique here is employed to study the transient absorption of MXene in solutions. In **Figure 1a**, we provided the schematic diagram of ultrafast pump-probe for interfacial energy transports at MXene surface with molecules. Because MXene has strong plasmonic absorption at 780 nm (Figure 1b), the pump frequency was set at 780 nm to create electronic excitation of MXene, generating the excitation energy. The following broad band white light as probe beam could detect transient ultrafast spectrums of plasmonic MXene at different time delays (Figure 1c). The responding peaks were shown at 510 and 950 nm respecting the decay of MXene's electronic excited states, which were decreasing with delay time (Figure 1c). As the temperature increases in Figure 1d, the transition dipole moments of $\text{Ti}_3\text{C}_2\text{T}_x$ change, resulting in new absorptions (510 nm) and bleachings (780 nm) in temperature difference spectrum (the measured high temperature spectrum minus room temperature spectrum). Because the spectral changes presented from pump-probe measurements are induced by the temperature increasing inside MXene, these changes should also be detected by comparing the temperature difference with the visible spectra of the same sample at different temperature. Figure 1e displays the temperature difference visible spectrum (spectrum at 50°C minus spectrum at 22°C , green) and pump-probe spectrum at 40 ps (red). The two curves are essentially identical, verifying that the spectral changes in pump probe spectra around 510 nm peak are originated from the temperature increase because of plasmonic excitation of MXene at 780 nm induced thermal generation. The amplitudes of the

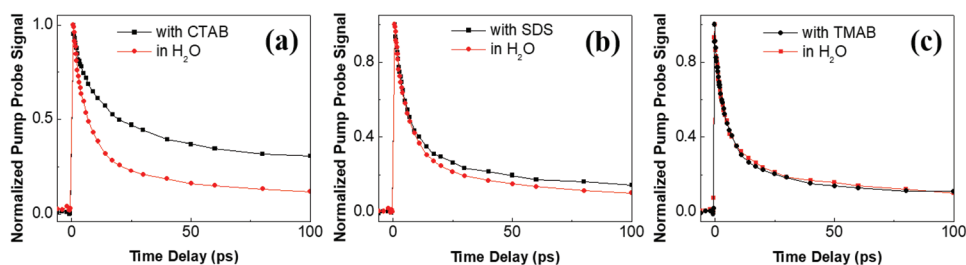


Figure 2. MXene dynamics in different surfactant solutions. a) MXene in CTAB solutions, b) MXene in SDS solutions, and c) MXene in TMAB solutions.

transition spectrum signal were proportional to the laser intensities without any line shape changing (Figure 1f). And different laser intensities could not alter the decay trends of the dynamics (Figure 1g). Thus, the ultrafast dynamics (pumping at 780 nm and probing at 510 nm) could provide the critical information for analyzing MXene energy dissipation in solutions.

2.2. CTAB Could Alter MXene Energy Decay Pathway Due to Strong Coulomb Interaction

We have chosen a set of molecular systems to examine the interfacial energy flow. Three types of organic molecules including two typical surfactant molecules (CTAB and SDS) and one control sample TMAB were added into MXene water solutions (0.05 mg mL^{-1}) respectively. The three typical molecules have different structural characteristics: CTAB has long hydrocarbon chain with positive charged quaternary ammonium head group; SDS has long hydrocarbon chain with negative charged sulfate

group; TMAB has positive head group but with short hydrocarbon chain. In this experiment, we detected the MXene ultrafast dynamics (pumping at 780 nm and probing at 510 nm) in these conditions in water with the dynamics of MXene in water alone without any additional molecule as the control experiment. As shown in Figure 2a, the addition of CTAB (0.2 mg mL^{-1}) could significantly retard MXene's excitation dynamics (black curve) compared with the dynamics of MXene in pure water solution (red curve). In contrast, SDS (0.5 mg mL^{-1}) and TMAB (0.5 mg mL^{-1}) could not dramatically change MXene ultrafast dynamic decay (Figure 2b,c, red and black curves are almost overlapped) and thus did not nearly generate influence on the MXene energy damping in the 100 ps time scale.

To understand the molecular origins of this energy damping difference, we then preformed coarse-grained molecular dynamics (CGMD) for the self-assembly of these three molecules in MXene-water solution system respectively. As shown in Figure 3a, CTAB molecules could

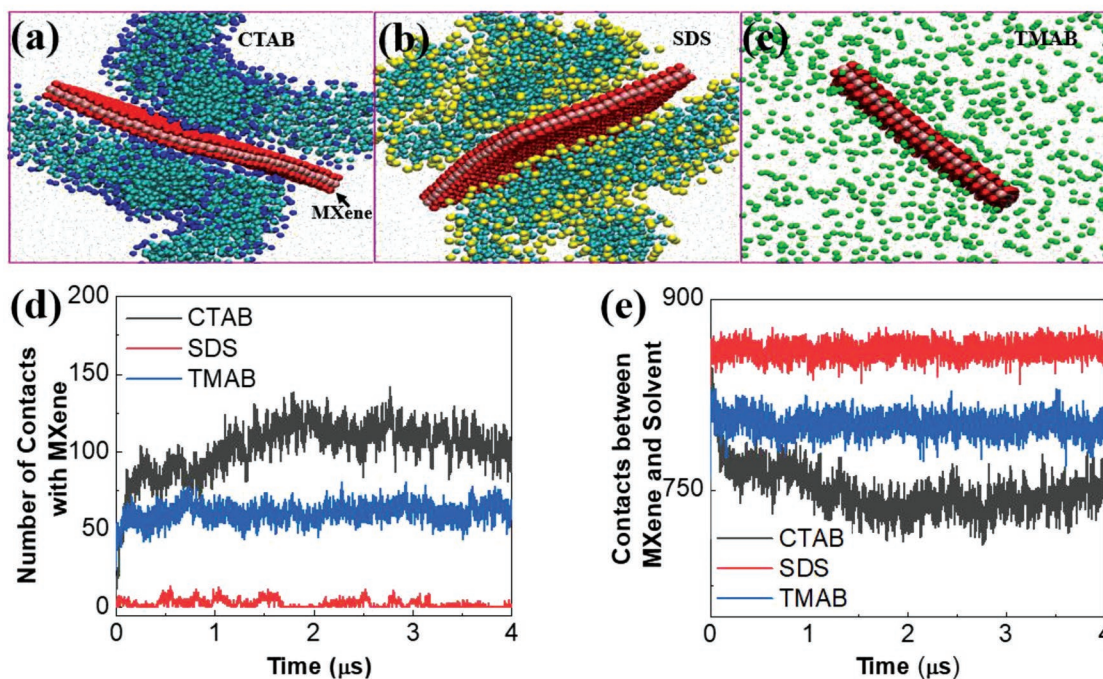


Figure 3. Self-assembly CGMD simulations of the aqueous mixture of MXene and CTAB/SDS/TMAB. CG snapshots of MXene ($9 \text{ nm} \times 9 \text{ nm}$), CTAB, SDS, and TMAB. Side-view system snapshots of MXene with a) CTAB, b) SDS, and c) TMAB at $t = 4 \text{ } \mu\text{s}$; MXene, CTAB, SDS, and TMAB are colored as (a), water/ions in gray points, simulation box in purple. d) Time evolution of contacts between MXene and CTAB/SDS/TMAB, e) between MXene and water/ions.

self-assemble into the bilayer-like structure, and tightly interact with the MXene surface, where water molecules were almost squeezed out completely from the MXene-bilayer interface. Similar with CTAB, SDS also formed the bilayer-like structure, but the MXene-bilayer interface was broken by the water molecules due to electrostatic repulsion between the MXene surface and SDS (Figure 3b). As for TMAB, they could diffuse much freely without the formation of the bilayer-like structure and adsorb partially on the MXene surface (Figure 3c). Further quantifications based on the contacts between MXene and CTAB/SDS/TMAB (Figure 3d) or water molecules (Figure 3e) well validated the aforementioned conclusions. Thus, we could observe that the SDS and TMAB could not effectively bypass the energy transport from MXene surface to water molecules. Even increasing the concentration of TMAB could not change the MXene's dynamics (Figure S1, Supporting Information). In principle, the $Ti_3C_2T_x$ flakes are negatively charged,^[32] and thus can attract positive charged CTAB to achieve close contact at the interfaces. The direct interaction between CTAB and MXene could provide the competing energy channel from MXene to surrounding molecules. Therefore, we could obtain the ultrafast dynamic differences as shown in Figure 2a. The results demonstrated that CTAB could be a suitable molecule for studying MXene-surfactant interfacial energy conduction.

2.3. CTAB Fully Covered MXene System is Suitable Model for Thermal Conductance Investigation

To quantitatively obtain suitable MXene-CTAB system to study energy conductance at interface, we subsequently added different concentrations of CTAB into MXene water solution (0.05 mg mL^{-1}) varying from 0 to 3 mg mL^{-1} . The addition of CTAB slightly decreased the absorption at 780 nm at 0.1 mg mL^{-1} (Figure 1b). We noticed that the CTAB critical micelle concentration (CMC) is around 0.3 mg mL^{-1} . The series of experiments could span the CMC point and thus be used to evaluate the binding ability of CTAB on MXene competing against CTAB self-assembly in water. In Figure 4a, we obtained the dynamics data on MXene solution with these different CTAB concentrations. Also we numerically fitted the dynamic data with bi-exponential decay function as $A = C_1 \exp(-t/T_1) + C_2 \exp(-t/T_2)$. The fitting parameters for different concentration CTAB were listed in Table S1 (Supporting Information). Obviously, the energy dissipation pathway could

be numerically described as fast part and slow part. Without the addition of CTAB, the 76.2% excitation energy could dissipate through the fast part around 5 ps, and the rest 23.8% excitation energy slowly damp to environment around 56 ps via the slow part. Gradually increasing CTAB concentrations, as shown in Figure 4b,c, both parts with different relaxation rates were altered. Initially, once CTAB binding on MXene surface with low concentration, it started to slightly retard MXene's energy relaxation rates. It's also noticed that with CTAB's addition, the slow part would take more energy. The transitions occurred for both parts at 0.1 mg mL^{-1} ranges. At transition point 0.1 mg mL^{-1} , 2/3 MXene energy loss would go with fast part with the time constant 8.89 ps, and 1/3 excitation energy of MXene would dissipate through slow part with the time constant 230.96 ps. Once exceeding the transition point 0.1 mg mL^{-1} , shown in Figure 4b,c, MXene energy relaxation rates for both parts would be faster. From our results, we found that the addition of 0.1 mg mL^{-1} CTAB would be the best candidate for capturing CTAB-MXene interfacial energy conductance.

To understand the complex MXene-CTAB structure in solution, we also need to consider two following assumptions together: 1) CTAB molecules need to form bilayers and be stabilized at $Ti_3C_2T_x$ flakes surfaces; 2) CTAB could symmetrically bind on each side of the $Ti_3C_2T_x$ flakes. With these assumptions, at transition point, we then take $Ti_3C_2T_x$ density^[32] as 3.19 g cm^{-3} and CTAB density^[25] as 1 g cm^{-3} to obtain the relative volume ratio ($Ti_3C_2T_x$ to CTAB) 1/6.38 in this solution ($Ti_3C_2T_x$ /CTAB mass ratio is $0.05/0.1 = 0.5$). At this concentration (0.1 g mL^{-1}), we roughly assumed that CTAB molecules just fully cover the $Ti_3C_2T_x$ surfaces. The ratio of $Ti_3C_2T_x$ single flake thickness ($\approx 1 \text{ nm}$)^[32] to CTAB bilayers thickness ($3.9 \text{ nm} \times 2$) should be 1/7.8. The area ratio (volume ratio/thickness ratio) of $Ti_3C_2T_x$ to CTAB is around 7.8/6.38. That means that if all $Ti_3C_2T_x$ are the single layer flakes, 0.1 mg mL^{-1} CTAB molecules are not enough to cover the surface area. Thus, 36% $Ti_3C_2T_x$ would pile up to two sheets to keep the area ratio of $Ti_3C_2T_x$ to CTAB as 1/1. Therefore, in the transition point 0.1 mg mL^{-1} , we obtained that in solution, 64% $Ti_3C_2T_x$ as single sheet interact with the double layer CTAB molecules, and the rest 36% $Ti_3C_2T_x$ should be stacked as double sheets symmetrically covered by two CTAB bilayers.

To understand the concentration dependent dynamics, we then performed all-atom simulation (AAMD). As shown in Figure 5, we tuned the CTAB area concentrations on MXene surface from 1.49 to 3.16 nm^{-2} . The three concentrations are corresponding to a) less occupancy, b) intermediate occupancy,

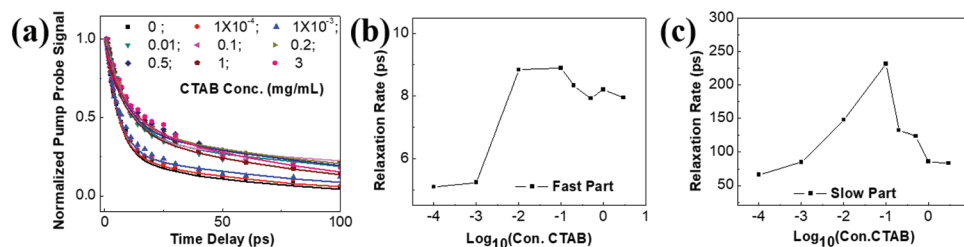


Figure 4. MXene dynamics in different concentration of CTAB. a) Pump-probe data of MXene in different concentration CTAB solutions, b) fast part decay rates, and c) slow part decay rates.

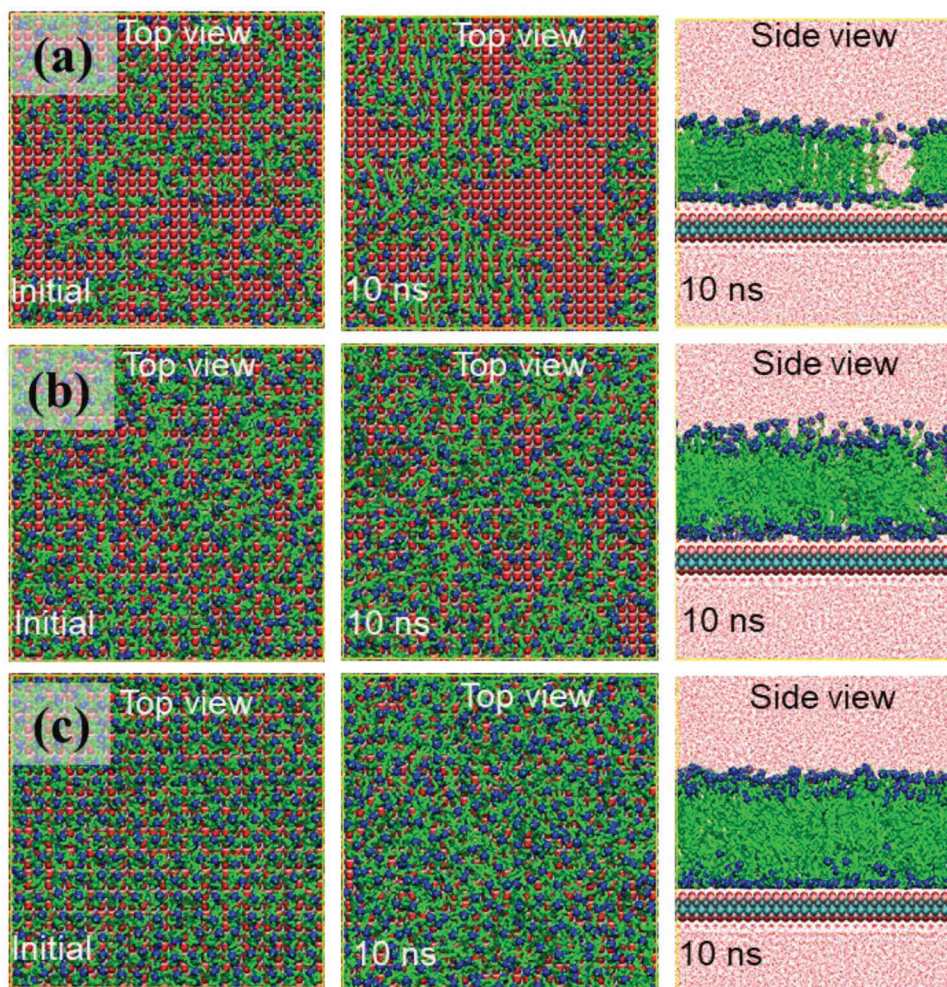


Figure 5. AAMD simulations of MXene-supported CTAB bilayers with different area concentrations: a) 1.49 nm^{-2} , b) 2.42 nm^{-2} , and c) 3.16 nm^{-2} . Left panel shows top-view snapshots of initial system setup. Middle panel and right panel show the top-view and side-view snapshots of the last frames of 10 ns AAMD simulations. MXene is shown in beads with the planar structure, CTAB in green licorice with charged head-groups in blue beads, water/ions in pink points.

and c) full occupancy. Initially, CTAB molecules are randomly distributed on MXene surfaces (left panels). After 10 ns, CTAB molecules would assemble into stable bilayer structures. As shown in top views (middle panels), different CTAB concentrations will expose different numbers of vacancies on the MXene surfaces. From side view (right panels), we could clearly see that increasing the CTAB concentration from (a) to (c) would block the water to bind on the surface and thus inhibit the energy dissipation through water channel directly. Therefore, the addition of CTAB before CMC point would take vacancies on MXene surfaces and thus retard the energy dissipation rate of MXene. After the transition point, more CTAB molecules would involve into self-assembled micelle structures. In this situation, MXene only might attach on the micelle surface and still expose some vacancies sites for water to bind with, shown in Figure 2a. Thus, it is reasonable that the MXene dynamics turned to faster values after 0.1 mg mL^{-1} CTAB concentration. Therefore, from molecular origins, the transition point concentration of CTAB-MXene system is appropriate to investigate quantitative interfacial thermal conductance for MXene.

2.4. Flash Energy Migration from MXene to CTAB

With this transition point, we could understand the energy dissipation pathway for MXene-CTAB interface. Generally, with absorption of resonance laser pump pulse, the first process for MXene as plasmonic material is the fast nonthermal internal equilibrium by electron–electron scattering. Then, for this flat 2D nanosheets, the electron–phonon coupling is within 2 ps. After this fast thermalization on the nanosheet, the fast out-plane energy transfer from MXene to the interface layer binding molecules occurs. This dynamic picture is quite different from the gold nanorod-CTAB interface, which has slower internal energy conversions (the ultrafast dynamics decay of gold nanorods at the first 10 ps is due to electron–phonon coupling, and is followed by thermal decay for $\approx 500 \text{ ps}$).^[25] Based on our results, this fast part time constant of energy transfer at interface is 8.89 ps. The thermal energy then dissipated along the hydrocarbon chains to the surrounding solvents. And the hydrocarbon heat transport contributes to the slow part. The time constant 230.96 ps obtained in the slow part is similar as

the reported^[18] heat loss time constant 250 ps from the micelle on carbon nanotube to the D₂O.

Based on this physical picture, we could calculate the interface energy conductance at Ti₃C₂T_x nanosheets surface based on the fast part with the Kapitza conductance^[33] as following: $G = Q/(A \times \tau \times \Delta T)$, where Q is the energy flux across the interface, τ is the energy flow time constant, G is the interface conductance, A is the interface area and, ΔT is the discontinuous temperature drop at the interface.^[34] In our case, the Q could be obtained based on the experimental parameters—light intensity and absorbance of MXene in CTAB/water solution. A could be calculated by combining MXene concentration in the light illumination area with Ti₃C₂T_x density^[32] 3.19 g cm⁻³. ΔT is difficult to directly be found out. Here, we took advantage of the heat capacity of TiC^[35] to calculate the initial temperature arising at MXene surface after electron–phonon coupling. According to the above experimental parameters, we could obtain the $\Delta T_{\text{interface}}$ of 100 K between MXene and CTAB as minimum energy drop. Based on these values, we could then calculate the interfacial energy conductance based on the fast part dynamics as 81.6 MW m⁻² K⁻¹ (detail calculations are in the Supporting Information). Also, the pioneer's work^[25] reported that before CMC concentration, the thermal conductivity of CTAB is 0.18–0.24 W m⁻¹ K⁻¹ and heat capacity is 2.0 J g⁻¹ K⁻¹. We thus calculated the thermal conducting time through 3.9–4.0 nm CTAB bilayer is around 221 ps, which is close to the slow part rate of 230.96 ps. Also, it is noticed that before the transition point, MXene dynamic with the addition of 0.01 g mL⁻¹ CTAB showed the fast part time constant 8.84 ps (Figure 4b), which is similar with the 8.89 ps in transition point. However, it showed nearly twice faster in the slow part time constant (100–150 ps) compared with the transition point (Figure 4c). This indicated that initial concentration of CTAB molecules on MXene might have one layer with the thickness of around 2 nm, and thus the thermal transfer costing time inside the chain is twice shorter than that in transition point. This CTAB concentration dependent layer altering phenomenon is also consistent with that on gold nanorod surface.^[25] Therefore, based on our thermal conductivity calculation, we could describe the entire physical process after fast electron–phonon coupling on MXene as following: the converted thermal energy would fast migrate through the MXene–CTAB interface with G 81 MW m⁻² K⁻¹ and time approximate to 10 ps, then the thermal energy would slowly transfer along the CTAB bilayers with the time constant around 221 ps.

It is surprising to notice that our obtained interfacial energy conductance value G of MXene–CTAB \approx 81 MW m⁻² K⁻¹ is significantly higher than that on MXene–AlO_x interface (<20 MW m⁻² K⁻¹). The results suggests that the soft CTAB could bond more tightly with MXene surface than hard AlO_x, which leads to a more efficient energy conduction across the interface.^[36] The MXene–CTAB interface G is also more prominent than the carbon material–surfactant/solvent interface such as CNT–SDS interface^[18] (\approx 10 MW m⁻² K⁻¹) and graphene–water interface^[37] (\approx 60 MW m⁻² K⁻¹). There are two reasons for this: 1) MXene (Ti₃C₂T_x) is plasmonic material with extremely fast electron–phonon coupling, and thus the phonon energy would quickly convert at this 2D flat interface; 2) MXene (Ti₃C₂T_x) surface is negatively charged and can form

ionic bond with CTAB head group, which is much stronger than the weak hydrogen bond and van der Waals interaction at interface, and thus results in more stable contact and rapid energy transduction. Nevertheless, our results are slightly lower than the thermal conductance values (130–450 MW m⁻² K⁻¹) of CTAB–Au nanorod interface in water obtained by the transition absorption approach, indicating that there might exists a more effective contact between CTAB and gold. Overall, attributed to the high near IR photo absorbance, advanced 2D flat surface and excellent interfacial conductivity, MXene–soft material would present brilliant future in thermal related applications.

2.5. Bilayer Surfactants Structures Could be Perturbed by Thermal Transport

The interfacial energy conduction from MXene to CTAB is fast, but the second interface conduction from CTAB to water is slow. Thus, the CTAB molecules in a short time scale (\approx 221 ps) would accumulate heat inside the structure. In the Supporting Information, we roughly calculate that the surface CTAB bilayers could elevate \approx 14 K inside the structure within 10 ps. We then employed AAMD simulation to investigate the CTAB structure under this flash thermal effect. As shown in Figure 6, rising the surface temperature from 295 K (left panels) to 350 K (right panels) would significantly increase the disorder of the CTAB structures. Pioneer's SFG work also experimentally confirmed this heating disordering phenomenon on SAM molecules.^[19] Therefore, our results indicate that flash heating

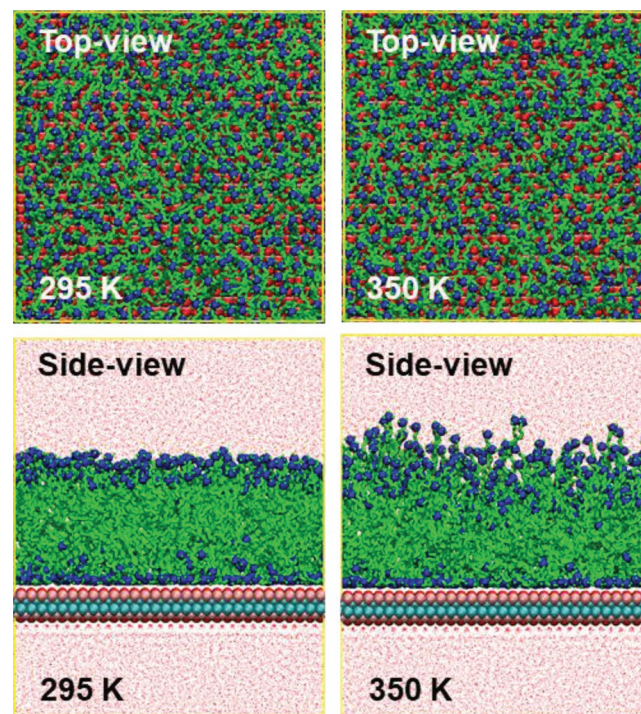


Figure 6. AAMD simulations of MXene-supported CTAB bilayers with the area concentrations of 3.16 nm⁻² at room temperature (295 K, left panel) and high temperature (350 K, right panel). Both top-view (upper row) and side-view (low row) snapshots of the simulation systems are shown here.

MXene by surface plasmonic resonance frequency laser would fast disturb the attached bilayer structures, showing the promising application in biomedical laser therapy.

3. Conclusion

In this work, we combined the ultrafast spectroscopy and MD simulation to investigate the way to tune the energy conduction pathway at MXene interface. With quantitatively studying the transient absorption dynamics, the surfactant molecule CTAB with strong coulomb interaction can form stable bilayers on MXene surface, and thus blocks the energy damping from MXene to water. By optimizing CTAB concentration for MXene energy dissipation, the thermal conductance of MXene-CTAB interface can achieve $\approx 81 \text{ MW m}^{-2} \text{ K}^{-1}$ which is within the typical range of conductance of soft plasmonic interfaces. Modeling the surfactant-MXene interaction can capture molecular origins of energy conduction at this interface. These findings and models lay the ground for future rational designs of MXene interfacial thermal applications, particularly for biomedical applications such as photothermal therapy treatments.

4. Experimental Section

Preparation of MXene ($\text{Ti}_3\text{C}_2\text{T}_x$): The preparation of MXene is similar with the previous report.^[31] In a typical synthesis, 1 g LiF was dissolved into 20 mL of 9 M hydrochloric acid, and then 1 g Ti_3AlC_2 powders (200 mesh) were added into the previous mixed solution and reacted at 35 °C for 24 h with a gentle stirring. Thereafter, the products were washed repeatedly with DI water by centrifugation of 3500 rpm (5 min for each cycle) until pH value excesses 6. To obtain highly dispersible MXene nanosheets, the supernatant after centrifugation was decanted, and the sediment was redispersed in DI water under manual shaking of 5 min. Then the dispersion solution was centrifuged at a low speed (typically 3500 rpm) for 20 min, and the resulting supernatant was collected for further characterization and test. Scanning electron microscope (SEM) picture is in Figure S2 (Supporting Information). MXene solids were obtained by vacuum filtration and subsequent freeze drying.

Preparation of Stable MXene Colloidal Solution: 1 mg MXene was dispersed in 20 mL aqueous solution and ultrasonicated (100 W, 20 min). Then, solution was centrifuged at 3500 rpm for 10 min twice to remove unstable suspensions, and finally stable MXene colloidal solution was obtained. The concentration of stable colloidal solution was measured by weighing the solids in a certain amount of dispersion solution after drying and then calculating their weight percentage. MXene's concentration is set at about 0.05 mg mL⁻¹ then CTAB with various mass is added when running the transient absorption experiment. The concentrations of SDS and TMAB in Figure 2 are both 0.5 mg mL⁻¹, and the concentration of CTAB in Figure 2 is 0.2 mg mL⁻¹.

Vis-NIR Ultrafast Transient Absorption Spectroscopy System: In this work, homemade femtosecond transient absorption system was employed. Briefly, the experiment setup is described as following: a broadband oscillator (Coherent Vitesse, 1 W) generates seed pulses of 20 fs duration with a wavelength of 800 nm, a bandwidth of 80 nm at a repetition rate of 80 MHz. The seed pulse is coupled into regenerative amplifier (Coherent Legend Elite HE+USP-1K-III). The output from the laser system is 35 fs pulse and 7 mJ with 10.5 mm of diameter, a center wavelength of 800 nm, a bandwidth of 40 nm with a repetition rate of 1 KHz. The laser was split into three beams. The first one was put into OPA (light conversion: Topas+UV/vis) to generate laser pulse of 240–2500 nm as pump beam with the pulse width of about 70–150 fs. In this experiment, the pump beam wavelength is set to be 780 nm with pulse energy 2 μJ . The pump spot diameter to be focused is about

400 μm by using a quartz lens (focusing length 750 mm). The second beam with weaker energy was focused on a sapphire plate to produce broadband white-light continuum pulses as probe pulses ranging from 450 to 1100 nm. A motorized delay stage was used to control the time delay between the pump and probe beams, both of which were focused onto the sample and overlapped spatially. After passing through the sample, the photoinduced transmission change of the probe light was collected by a fiber spectrometer (AvaSpec-ULS2048CL-EVO, Avantes). A magnetic stirring was applied to stir sample in order to avoid the sample damage under laser illumination.

Molecular Dynamics Simulations: MD simulation has been proven to be a powerful tool in studying the interactions between 2D nanomaterials and small organic molecules.^[38,39] In this work, Martini coarse-grained (CG) force field (version 2.1)^[40] and CHARMM36m all-atom (AA) force field^[41] were used to capture the dynamics of CTAB, SDS, and TMAB on the surface of MXene ($\text{Ti}_3\text{C}_2\text{O}_2$). The chemical structure and parameters of MXene are adapted or modified from the previous researches.^[42,43] For all simulations, GROMACS software (version 2016.5) and suggested parameters for each force field were used. The self-assembly processes of these three surfactant molecules on MXene were simulated by CGMD simulations. Each CGMD simulation contained one 9 nm \times 9 nm MXene sheet and 806 CTAB/SDS/TMAB molecules, and was run for 4 μs with the time step of 20 fs. The molecular details of packing defects due to the adsorption density of CTAB molecules and the local temperature were further studied by AAMD simulations. Each AAMD simulation contained one 9 nm \times 9 nm MXene sheet and 242/392/512 CTAB molecules, and was run for 10 ns with the time step of 2 fs.

Supporting Information

Supporting Information is available from the Wiley Online Library or from the author.

Acknowledgements

J.L. and Q.Z. contributed equally to this work. This work is supported by National Natural Science Foundation of China (NSFC-21803006 and NSFC-51702009) and the Fundamental Research Funds for the Central Universities. M.H. also thanks to the National Natural Science Foundation of China (21771017). K.Y. also thanks to the National Natural Science Foundation of China (21873099 and 21673232).

Conflict of Interest

The authors declare no conflict of interest.

Keywords

interfacial thermal conductance, MXene, photothermal, surfactants, ultrafast

Received: August 21, 2019
Revised: September 18, 2019
Published online:

- [1] E. Yalon, C. J. McClellan, K. K. Smithe, M. Muñoz Rojo, R. L. Xu, S. V. Suryavanshi, A. J. Gabourie, C. M. Neumann, F. Xiong, A. B. Farimani, *Nano Lett.* **2017**, *17*, 3429.
- [2] X. Xu, N. M. Gabor, J. S. Alden, A. M. van der Zande, P. L. McEuen, *Nano Lett.* **2010**, *10*, 562.

- [3] A. M. Gobin, M. H. Lee, N. J. Halas, W. D. James, R. A. Drezek, J. L. West, *Nano Lett.* **2007**, *7*, 1929.
- [4] H. Song, J. Liu, B. Liu, J. Wu, H.-M. Cheng, F. Kang, *Joule* **2018**, *2*, 442.
- [5] A. L. Moore, L. Shi, *Mater. Today* **2014**, *17*, 163.
- [6] L. Fan, J. M. Khodadadi, *Renewable Sustainable Energy Rev.* **2011**, *15*, 24.
- [7] X. Wei, T. Zhang, T. Luo, *ACS Energy Lett.* **2017**, *2*, 2283.
- [8] Y. Wang, Z. Qin, M. J. Buehler, Z. Xu, *Nat. Commun.* **2016**, *7*, 12854.
- [9] J. K. El-Demellawi, S. Lopatin, J. Yin, O. F. Mohammed, H. N. Alshareef, *ACS Nano* **2018**, *12*, 8485.
- [10] K. Hantanasirisakul, Y. Gogotsi, *Adv. Mater.* **2018**, *30*, 1804779.
- [11] R. Li, L. Zhang, L. Shi, P. Wang, *ACS Nano* **2017**, *11*, 3752.
- [12] C. Yang, D. Xu, W. Peng, Y. Li, G. Zhang, F. Zhang, X. Fan, *Nanoscale* **2018**, *10*, 15387.
- [13] J. Peng, X. Chen, W.-J. Ong, X. Zhao, N. Li, *Chem* **2019**, *5*, 18.
- [14] C. Dai, Y. Chen, X. Jing, L. Xiang, D. Yang, H. Lin, Z. Liu, X. Han, R. Wu, *ACS Nano* **2017**, *11*, 12696.
- [15] C. Xing, S. Chen, X. Liang, Q. Liu, M. Qu, Q. Zou, J. Li, H. Tan, L. Liu, D. Fan, *ACS Appl. Mater. Interfaces* **2018**, *10*, 27631.
- [16] X. Han, J. Huang, H. Lin, Z. Wang, P. Li, Y. Chen, *Adv. Healthcare Mater.* **2018**, *7*, 1701394.
- [17] C. Dai, H. Lin, G. Xu, Z. Liu, R. Wu, Y. Chen, *Chem. Mater.* **2017**, *29*, 8637.
- [18] S. T. Huxtable, D. G. Cahill, S. Shenogin, L. Xue, R. Ozisik, P. Barone, M. Usrey, M. S. Strano, G. Siddons, M. Shim, *Nat. Mater.* **2003**, *2*, 731.
- [19] Z. Wang, J. A. Carter, A. Lagutchev, Y. K. Koh, N.-H. Seong, D. G. Cahill, D. D. Klott, *Science* **2007**, *317*, 787.
- [20] F. Sun, T. Zhang, M. M. Jobbins, Z. Guo, X. Zhang, Z. Zheng, D. Tang, S. Ptasinska, T. Luo, *Adv. Mater.* **2014**, *26*, 6093.
- [21] Z. Ge, D. G. Cahill, P. V. Braun, *Phys. Rev. Lett.* **2006**, *96*, 186101.
- [22] S. Hassan, M. Schade, C. P. Shaw, R. I. Lévy, P. Hamm, *J. Phys. Chem. B* **2014**, *118*, 7954.
- [23] J. Park, D. G. Cahill, *J. Phys. Chem. C* **2016**, *120*, 2814.
- [24] A. J. Schmidt, J. D. Alper, M. Chiesa, G. Chen, S. K. Das, K. Hamad-Schifferli, *J. Phys. Chem. C* **2008**, *112*, 13320.
- [25] J. Huang, J. Park, W. Wang, C. J. Murphy, D. G. Cahill, *ACS Nano* **2013**, *7*, 589.
- [26] X. Wu, Y. Ni, J. Zhu, N. D. Burrows, C. J. Murphy, T. Dumitrica, X. Wang, *ACS Appl. Mater. Interfaces* **2016**, *8*, 10581.
- [27] R. Bian, R. Lin, G. Wang, G. Lu, W. Zhi, S. Xiang, T. Wang, P. S. Clegg, D. Cai, W. Huang, *Nanoscale* **2018**, *10*, 3621.
- [28] Z. Li, H. Zhang, J. Han, Y. Chen, H. Lin, T. Yang, *Adv. Mater.* **2018**, *30*, 1706981.
- [29] M. Soleymaniha, M. A. Shahbazi, A. R. Rafeerad, A. Maleki, A. Amiri, *Adv. Healthcare Mater.* **2019**, *8*, 1801137.
- [30] J. Luo, W. Zhang, H. Yuan, C. Jin, L. Zhang, H. Huang, C. Liang, Y. Xia, J. Zhang, Y. Gan, *ACS Nano* **2017**, *11*, 2459.
- [31] J. Li, R. Qin, L. Yan, Z. Chi, Z. Yu, N. Li, M. Hu, H. Chen, G. Shan, *Inorg. Chem.* **2019**, *58*, 7285.
- [32] Z. Ling, C. E. Ren, M.-Q. Zhao, J. Yang, J. M. Giammarco, J. Qiu, M. W. Barsoum, Y. Gogotsi, *Proc. Natl. Acad. Sci. USA* **2014**, *111*, 16676.
- [33] E. T. Swartz, R. O. Pohl, *Rev. Mod. Phys.* **1989**, *61*, 605.
- [34] D. G. Cahill, P. V. Braun, G. Chen, D. R. Clarke, S. Fan, K. E. Goodson, P. Keblinski, W. P. King, G. D. Mahan, A. Majumdar, *Appl. Phys. Rev.* **2014**, *1*, 011305.
- [35] J. F. Shackelford, W. Alexander, *CRC Materials Science and Engineering Handbook*, CRC press LLC, Boca Raton, FL **2001**.
- [36] P. Yasaei, Z. Hemmat, C. J. Foss, S. J. Li, L. Hong, A. Behranginia, L. Majidi, R. F. Klie, M. W. Barsoum, Z. Aksamija, *Adv. Mater.* **2018**, *30*, 1801629.
- [37] D. Alexeev, J. Chen, J. H. Walther, K. P. Giapis, P. Angelikopoulos, P. Koumoutsakos, *Nano Lett.* **2015**, *15*, 5744.
- [38] Z. Li, Y. Zhang, C. Chan, C. Zhi, X. Cheng, J. Fan, *ACS Nano* **2018**, *12*, 2764.
- [39] Y. Tu, M. Lv, P. Xiu, T. Huynh, M. Zhang, M. Castelli, Z. Liu, Q. Huang, C. Fan, H. Fang, *Nat. Nanotechnol.* **2013**, *8*, 594.
- [40] S. J. Marrink, H. J. Risselada, S. Yefimov, D. P. Tieleman, A. H. De Vries, *J. Phys. Chem. B* **2007**, *111*, 7812.
- [41] J. Huang, S. Rauscher, G. Nawrocki, T. Ran, M. Feig, B. L. de Groot, H. Grubmüller, A. D. MacKerell Jr., *Nat. Methods* **2017**, *14*, 71.
- [42] M. Khazaei, M. Arai, T. Sasaki, C. Y. Chung, N. S. Venkataramanan, M. Estili, Y. Sakka, Y. Kawazoe, *Adv. Funct. Mater.* **2013**, *23*, 2185.
- [43] L. Ding, Y. Wei, L. Li, T. Zhang, H. Wang, J. Xue, L.-X. Ding, S. Wang, J. Caro, Y. Gogotsi, *Nat. Commun.* **2018**, *9*, 155.